Journal of Innovative Optical Health Sciences
Vol. 7, No. 1 (2014) 1450013 (9 pages)

DOI: 10.1142/S1793545814500138

World Scientific
www.worldscientific.com

COHERENT HEMODYNAMICS SPECTROSCOPY BASED ON A PACED BREATHING PARADIGM — REVISITED

JANA M. KAINERSTORFER*, ANGELO SASSAROLI,
MICHELE L. PIERRO, BERTAN HALLACOGLU†
and SERGIO FANTINI
Department of Biomedical Engineering, Tufts University
4 Colby Street, Medford, MA 02155, USA
**jana.kainerstorfer@tufts.edu*

Received 2 October 2013
Accepted 27 November 2013
Published 20 January 2014

A novel hemodynamic model has been recently introduced, which provides analytical relationships between the changes in cerebral blood volume (CBV), cerebral blood flow (CBF), and cerebral metabolic rate of oxygen ($CMRO_2$), and associated changes in the tissue concentrations of oxy- and deoxy-hemoglobin (ΔO and ΔD) measured with near-infrared spectroscopy (NIRS) [S. Fantini, *Neuroimage* **85**, 202–221 (2014)]. This novel model can be applied to measurements of the amplitude and phase of induced hemodynamic oscillations as a function of the frequency of oscillation, realizing the novel technique of coherent hemodynamics spectroscopy (CHS) [S. Fantini, *Neuroimage* **85**, 202–221 (2014); M. L. Pierro *et al.*, *Neuroimage* **85**, 222–233 (2014)]. In a previous work, we have demonstrated an *in vivo* application of CHS on human subjects during paced breathing [M. L. Pierro *et al.*, *Neuroimage* **85**, 222–233 (2014)]. In this work, we present a new analysis of the collected data during paced breathing based on a slightly revised formulation of the hemodynamic model and an efficient fitting procedure. While we have initially treated all 12 model parameters as independent, we have found that, in this new implementation of CHS, the number of independent parameters is eight. In this article, we identify the eight independent model parameters and we show that our previous results are consistent with the new formulation, once the individual parameters of the earlier analysis are combined into the new set of independent parameters.

Keywords: Hemodynamic model; near-infrared spectroscopy; cerebral autoregulation; cerebral blood flow; metabolic rate of oxygen.

†Current affiliation: Cephalogics, LLC, 33 Arch Street Suite 3201 Boston, MA 02110, USA

1. Introduction

Cerebral hemodynamics can be measured with near-infrared spectroscopy (NIRS). For example, functional brain studies with NIRS, or fNIRS, based on hemodynamic changes associated with cognitive or task-related brain activation have been reported numerous times.[3–5] The underlying physiological mechanisms of such hemodynamic changes are related to the cerebral blood flow (CBF), cerebral blood volume (CBV) and cerebral metabolic rate of oxygen ($CMRO_2$). In addition to hemodynamic changes associated with brain activation, spontaneous hemodynamic fluctuations have also been reported. In particular, spontaneous low frequency oscillations (LFOs) (at frequencies $\lesssim 0.1$ Hz) have been observed, reflecting a combination of systemic cardiovascular dynamics and local metabolic and flow regulation effects.[6] While low frequency oscillations occur spontaneously, cerebral hemodynamic oscillations can also be induced at a specific frequency. Protocols for inducing cerebral hemodynamic oscillations include paced breathing,[7] periodic head-uptilting,[8] repeated squat-stand,[9] a sit-stand maneuvers,[10] and cyclic pneumatic thigh-cuff inflation.[11]

A quantitative relationship between induced hemodynamic oscillations and the underlying CBF, CBV, and $CMRO_2$ oscillations was recently obtained by a novel hemodynamic model introduced by Fantini.[1,12] The model shows that measured total hemoglobin oscillations are directly linked to blood volume oscillations, while phase differences between oxy- and deoxy- hemoglobin oscillations are indicative of CBF and $CMRO_2$ changes. This hemodynamic model, together with measurements of hemodynamic oscillations at multiple frequencies, lead to the novel technique of coherent hemodynamics spectroscopy (CHS) that we have recently proposed[1] and demonstrated on human subjects.[2] CHS allows for the determination of a set of physiological parameters related to the blood transit time in the microvasculature, microvascular blood volume, and autoregulation. We have shown previously that this method can be applied to NIRS data collected during a paced breathing paradigm, where cerebral hemodynamic oscillations were induced at multiple frequencies by varying the respiratory rate.[2] We have also shown that the data, namely the amplitude ratios of deoxy- and oxy-hemoglobin phasors, $|\mathbf{D}|/|\mathbf{O}|$, oxy- and total-hemoglobin phasors, $|\mathbf{O}|/|\mathbf{T}|$, as well as the phase differences between them, $\arg(\mathbf{D})$–$\arg(\mathbf{O})$, and $\arg(\mathbf{O})$–$\arg(\mathbf{T})$, can be well fit with the hemodynamic model by Fantini.[1,2] The resulting fits yielded the values of ten physiological parameters (two parameters were set at fixed values). While the solutions did fit the hemodynamic spectra well, we recently found that the solutions of the physiological parameters were not unique[13] due to the lack of independence between some of them. Here, we revisit the paced breathing data set and apply a slightly revised formulation of the model with a reduced set of eight independent parameters. We demonstrate that the previously published solutions are consistent with the new set of independent model parameters.

2. Methods

2.1. *Experimental methods and paced breathing protocol for coherent hemodynamics spectroscopy*

The methods of obtaining frequency resolved spectra of hemodynamic oscillations (CHS) and the experimental setup for the paced breathing protocol have been described previously.[1,2] NIRS measurements were performed with a commercial tissue oximeter (OxiplexTS, ISS, Inc., Champaign, IL) at a detection sampling rate of 6.25 Hz at two wavelengths, 690 and 830 nm. Eleven subjects participated in a paced breathing paradigm, with the optical probe placed on the right side of their forehead and held in place by a flexible headband. Continuous monitoring of respiration was done with a strain gauge placed around the subject's chest, connected to an auxiliary input port of the tissue spectrometer for simultaneous recording with the optical data. Eleven healthy adult volunteers (numbered 1–11), five males (subjects Nos. 1, 2, 3, 4, 6) and six females (subjects Nos. 5, 7, 8, 9, 10, 11), participated in the study. Five subjects (Nos. 1–5) performed paced breathing at 11 frequencies (0.071, 0.077, 0.083, 0.091, 0.100, 0.111, 0.125, 0.143, 0.167, 0.200, 0.250 Hz) for a total time of 2 min per frequency. Six subjects (Nos. 6–11) performed paced breathing at four frequencies (0.071, 0.100, 0.167, 0.250 Hz) for a total time of 5 min per frequency. All subjects were prompted by a breathing metronome to guide them through the inhalation and exhalation phases of paced breathing. The experimental protocol was approved by the Tufts University Institutional Review Board (IRB) and written informed consent was obtained from all participants prior to the study.

2.2. *Data analysis*

2.2.1. *Pre-processing*

The optical data at 690 and 830 nm were translated into deoxy-hemoglobin (D) and oxy-hemoglobin (O) concentrations by utilizing the modified Beer–Lambert law. Slow temporal drifts were removed from the data with a third order polynomial detrending. Linear bandpass filtering was performed around each paced breathing frequency based on the Parks–McClellan algorithm with the width of the bandpass being 0.02 Hz. Using this band pass filtered data, we expressed the D and O oscillations at a given frequency ω in terms of phasors $\mathbf{O}(\omega)$ and $\mathbf{D}(\omega)$. We then obtained the amplitude ratios $|\mathbf{D}|/|\mathbf{O}|$, $|\mathbf{O}|/|\mathbf{T}|$, and the phase differences $\arg(\mathbf{D})$–$\arg(\mathbf{O})$ and $\arg(\mathbf{O})$–$\arg(\mathbf{T})$ for each paced breathing frequency. Here, we perform a new analysis of previously collected paced breathing data[2] by using a modified formulation (described below) of the hemodynamic model introduced by Fantini.[12,13]

2.2.2. *The hemodynamic model*

The new hemodynamic model by Fantini[1] describes sinusoidal oscillations of the cerebral concentrations of oxy- and deoxy-hemoglobin as the output of a linear time invariant system for which oscillations in CBV, CBF, and $CMRO_2$ act as input parameters. The oscillatory hemoglobin concentrations and physiological parameters are represented by phasors that are indicated in bold face. The model expresses $\mathbf{O}(\omega)$, $\mathbf{D}(\omega)$, and $\mathbf{T}(\omega)$ (i.e., the phasors that describe the oscillations of oxy-, deoxy- and total hemoglobin concentrations, respectively) as a function of $\mathbf{cbv}(\omega)$, $\mathbf{cbf}(\omega)$, and $\mathbf{cmro_2}(\omega)$ (i.e. phasors that describe the oscillations of CBV, CBF, and $CMRO_2$, respectively).[12] We have shown previously[1,2,12,13] that taking amplitude ratios and phase differences between hemoglobin phasors minimizes the sensitivity to the frequency dependence of the amplitude and phase of the source of induced hemoglobin oscillations (paced breathing in this study). The phasor ratios of deoxy-to-oxy hemoglobin concentrations, and oxy-to-total hemoglobin concentrations[12] are:

$$\frac{\mathbf{D}(\omega)}{\mathbf{O}(\omega)} = \frac{|\mathbf{D}(\omega)|}{|\mathbf{O}(\omega)|} e^{i\{\mathrm{Arg}[\mathbf{D}(\omega)]-\mathrm{Arg}[\mathbf{O}(\omega)]\}} \left((1-S^{(a)}) \frac{\mathrm{CBV}_0^{(a)}\mathbf{cbv}^{(a)}(\omega)}{\mathrm{CBV}_0^{(v)}\mathbf{cbv}^{(v)}(\omega)} + (1-S^{(v)}) - \left[\frac{\langle S^{(c)}\rangle}{S^{(v)}} (\langle S^{(c)}\rangle - S^{(v)}) \mathcal{F}^{(c)} \frac{\mathrm{CBV}_0^{(c)}}{\mathrm{CBV}_0^{(v)}} \mathcal{H}^{(c)}_{\mathrm{RC-LP}}(\omega) + (S^{(a)} - S^{(v)}) \mathcal{H}^{(v)}_{\mathrm{G-LP}}(\omega) \right] \times k \frac{\mathrm{CBV}_0^{(v)}}{\mathrm{CBV}_0} \mathcal{H}^{(\mathrm{AutoReg})}_{\mathrm{RC-HP}}(\omega) \left[\frac{\mathrm{CBV}_0^{(a)}\mathbf{cbv}^{(a)}(\omega)}{\mathrm{CBV}_0^{(v)}\mathbf{cbv}^{(v)}(\omega)} + 1 \right] \right) = \frac{\left(S^{(a)} \frac{\mathrm{CBV}_0^{(a)}\mathbf{cbv}^{(a)}(\omega)}{\mathrm{CBV}_0^{(v)}\mathbf{cbv}^{(v)}(\omega)} + S^{(v)} + \left[\frac{\langle S^{(c)}\rangle}{S^{(v)}} (\langle S^{(c)}\rangle - S^{(v)}) \mathcal{F}^{(c)} \frac{\mathrm{CBV}_0^{(c)}}{\mathrm{CBV}_0^{(v)}} \mathcal{H}^{(c)}_{\mathrm{RC-LP}}(\omega) + (S^{(a)} - S^{(v)}) \mathcal{H}^{(v)}_{\mathrm{G-LP}}(\omega) \right] \times k \frac{\mathrm{CBV}_0^{(v)}}{\mathrm{CBV}_0} \mathcal{H}^{(\mathrm{AutoReg})}_{\mathrm{RC-HP}}(\omega) \left[\frac{\mathrm{CBV}_0^{(a)}\mathbf{cbv}^{(a)}(\omega)}{\mathrm{CBV}_0^{(v)}\mathbf{cbv}^{(v)}(\omega)} + 1 \right] \right)}{\left(\frac{\mathrm{CBV}_0^{(a)}\mathbf{cbv}^{(a)}(\omega)}{\mathrm{CBV}_0^{(v)}\mathbf{cbv}^{(v)}(\omega)} + 1 \right)}, \quad (1)$$

$$\frac{\mathbf{O}(\omega)}{\mathbf{T}(\omega)} = \frac{|\mathbf{O}(\omega)|}{|\mathbf{T}(\omega)|} e^{i\{\mathrm{Arg}[\mathbf{O}(\omega)]-\mathrm{Arg}[\mathbf{T}(\omega)]\}} \left(S^{(a)} \frac{\mathrm{CBV}_0^{(a)}\mathbf{cbv}^{(a)}(\omega)}{\mathrm{CBV}_0^{(v)}\mathbf{cbv}^{(v)}(\omega)} + S^{(v)} + \left[\frac{\langle S^{(c)}\rangle}{S^{(v)}} (\langle S^{(c)}\rangle - S^{(v)}) \mathcal{F}^{(c)} \frac{\mathrm{CBV}_0^{(c)}}{\mathrm{CBV}_0^{(v)}} \mathcal{H}^{(c)}_{\mathrm{RC-LP}}(\omega) + (S^{(a)} - S^{(v)}) \mathcal{H}^{(v)}_{\mathrm{G-LP}}(\omega) \right] \times k \frac{\mathrm{CBV}_0^{(v)}}{\mathrm{CBV}_0} \mathcal{H}^{(\mathrm{AutoReg})}_{\mathrm{RC-HP}}(\omega) \left[\frac{\mathrm{CBV}_0^{(a)}\mathbf{cbv}^{(a)}(\omega)}{\mathrm{CBV}_0^{(v)}\mathbf{cbv}^{(v)}(\omega)} + 1 \right] \right) = \frac{\left(S^{(a)} \frac{\mathrm{CBV}_0^{(a)}\mathbf{cbv}^{(a)}(\omega)}{\mathrm{CBV}_0^{(v)}\mathbf{cbv}^{(v)}(\omega)} + S^{(v)} + \left[\frac{\langle S^{(c)}\rangle}{S^{(v)}} (\langle S^{(c)}\rangle - S^{(v)}) \mathcal{F}^{(c)} \frac{\mathrm{CBV}_0^{(c)}}{\mathrm{CBV}_0^{(v)}} \mathcal{H}^{(c)}_{\mathrm{RC-LP}}(\omega) + (S^{(a)} - S^{(v)}) \mathcal{H}^{(v)}_{\mathrm{G-LP}}(\omega) \right] \times k \frac{\mathrm{CBV}_0^{(v)}}{\mathrm{CBV}_0} \mathcal{H}^{(\mathrm{AutoReg})}_{\mathrm{RC-HP}}(\omega) \left[\frac{\mathrm{CBV}_0^{(a)}\mathbf{cbv}^{(a)}(\omega)}{\mathrm{CBV}_0^{(v)}\mathbf{cbv}^{(v)}(\omega)} + 1 \right] \right)}{\left(\frac{\mathrm{CBV}_0^{(a)}\mathbf{cbv}^{(a)}(\omega)}{\mathrm{CBV}_0^{(v)}\mathbf{cbv}^{(v)}(\omega)} + 1 \right)}, \quad (2)$$

where $\mathcal{H}^{(c)}_{\mathrm{RC-LP}}(\omega)$ and $\mathcal{H}^{(v)}_{\mathrm{G-LP}}(\omega)$ are the capillary and venous complex transfer function, $S^{(a)}$, $\langle S^{(c)}\rangle$, $S^{(v)}$, are the arterial, capillary, and venous saturations, respectively, and $\mathcal{F}^{(c)}$ is the Fåhraeus

factor (ratio of capillary-to-large vessel hematocrit). The superscripts (a), (c), and (v) for CBV and **cbv** indicate partial contributions from the arterial, capillary, and venous compartments, respectively, with $\mathrm{CBV}_0 = \mathrm{CBV}_0^{(a)} + \mathrm{CBV}_0^{(c)} + \mathrm{CBV}_0^{(v)}$, where CBV_0 is the baseline blood volume concentration. We assume that the blood volumes of the arterial and venous compartments have the same frequency dependence, and we take the phase of blood volume oscillations as the phase reference. In other words, we set $\mathbf{cbv}^{(a)}(\omega) = \mathrm{cbv}^{(a)}(\omega)\angle 0^\circ$ and $\mathbf{cbv}^{(v)}(\omega) = \mathrm{cbv}^{(v)}(\omega)\angle 0^\circ$, and the phasor ratio $\mathbf{cbv}^{(a)}(\omega)/\mathbf{cbv}^{(v)}(\omega)$ is replaced by the real constant $\mathrm{cbv}^{(a)}/\mathrm{cbv}^{(v)}$ in Eqs. (1) and (2). Furthermore, it was assumed that induced hemodynamic oscillations do not involve modulation of the cerebral metabolic rate of oxygen, therefore $\mathbf{cmro_2}(\omega) = 0$. Since there is negligible dynamic dilation and recruitment of capillaries in brain tissue,[14–19] we have set $\mathbf{cbv}^{(c)}(\omega) = 0$. The following relationship between **cbf** and **cbv**[1] has been used to derive Eqs. (1) and (2):

$$\begin{aligned}\mathbf{cbf}(\omega) &= k\mathcal{H}_{\mathrm{RC-HP}}^{(\mathrm{AutoReg})}(\omega)\mathbf{cbv}(\omega)\\ &= k\mathcal{H}_{\mathrm{RC-HP}}^{(\mathrm{AutoReg})}(\omega)\left[\frac{\mathrm{CBV}_0^{(a)}}{\mathrm{CBV}_0}\mathbf{cbv}^{(a)}(\omega)\right.\\ &\quad\left.+\frac{\mathrm{CBV}_0^{(v)}}{\mathrm{CBV}_0}\mathbf{cbv}^{(\mathrm{v})}(\omega)\right] \qquad (3)\end{aligned}$$

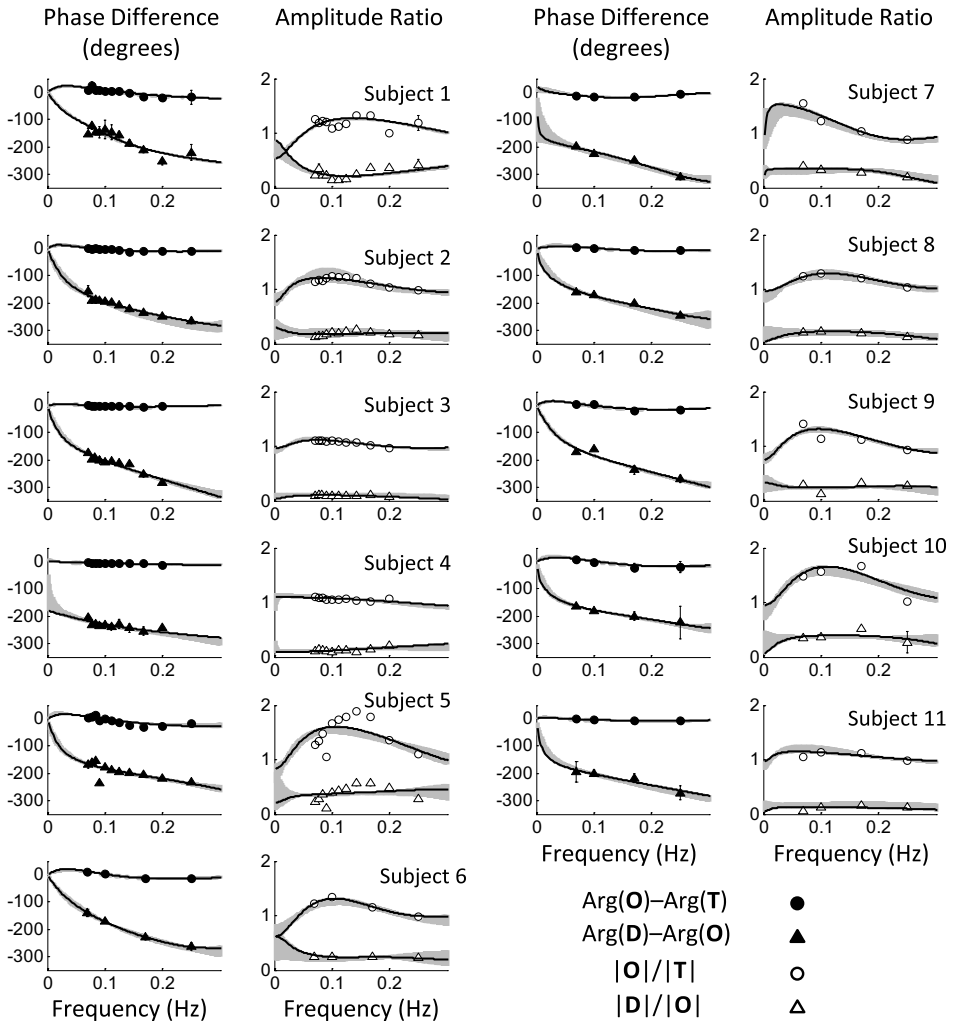

Fig. 1. Measured CHS spectra of all eleven subjects (symbols), and best fits obtained with the hemodynamic model (lines), as well as all solutions within one standard deviations of the experimental data (shaded area) for all eleven subjects. For each subject, the right panel shows the amplitude ratio spectra ratio spectra ($|\mathbf{O}|/|\mathbf{T}|$ and $|\mathbf{D}|/|\mathbf{O}|$), and the left panel shows the phase difference spectra (Arg(**O**)–Arg(**T**) and Arg(**D**)–Arg(**O**)).

where k is the inverse of the modified Grubb exponent, and $\mathcal{H}_{\mathrm{RC-HP}}^{(\mathrm{AutoReg})}(\omega)$ is the RC high-pass transfer function with cutoff frequency $\omega_c^{(\mathrm{AutoReg})}$ that describes the effect of autoregulation. In Eq. (3), we have assumed that $\mathbf{cbv}(\omega)$ is representative of arterial blood pressure oscillations, so that Eq. (3) provides a model of cerebral autoregulation.

In general, the model parameters are $S^{(a)}$, the arterial saturation, α, the rate constant for oxygen diffusion, $t^{(c)}$, blood transit time in capillaries, $t^{(v)}$, blood transit time in veins, $\mathrm{CBV}_0^{(a)}$, $\mathcal{F}^{(c)}\mathrm{CBV}_0^{(c)}$, $\mathrm{CBV}_0^{(v)}$, the baseline arterial, capillary (with Fåhraeus factor, $\mathcal{F}^{(c)}$, correction), and venous blood volume respectively, $\mathrm{cbv}^{(a)}$, $\mathrm{cbv}^{(c)}$, $\mathrm{cbv}^{(v)}$, the arterial, capillary, and venous blood volume amplitudes of oscillations, $\omega_c^{(\mathrm{AutoReg})}$, the autoregulation cutoff frequency, and k, the asymptotic flow-to-volume amplitude ratio. Assuming $S^{(a)}$ and α to be known, the number of unknown parameters is 10. We have shown previously that CHS spectra can be fitted and solutions can be found for those ten unknown parameters.[2] While solutions were obtained for all parameters, the fits required manual adjustments and the solutions did not necessarily correspond to the one yielding the smallest χ^2 value. Furthermore, we have recently shown that the solutions for these 10 parameters are not unique because some of those parameters are not independent from each other.[13] Specifically, in addition to setting $\mathbf{cbv}^{(c)}(\omega) = 0$, we have found that the model parameters can be reduced to the following set of eight independent parameters: $S^{(a)}$, α, $t^{(c)}$, $t^{(v)}$, $\mathcal{F}^{(c)}\mathrm{CBV}_0^{(c)}/\mathrm{CBV}_0^{(v)}$, $(\mathrm{CBV}_0^{(a)}\mathrm{cbv}^{(a)})/(\mathrm{CBV}_0^{(v)}\mathrm{cbv}^{(v)})$, $\omega_c^{(\mathrm{AutoReg})}$, and $k\mathrm{CBV}_0^{(v)}/\mathrm{CBV}_0$. After assuming a fixed value for the arterial saturation (98%) and setting $\alpha = 0.8\,\mathrm{s}^{-1}$, the number of unknown parameters can therefore be reduced to six. Additionally, given the independence of these parameters, we have improved the inversion procedure of the fits, yielding the best solution corresponding to the smallest possible χ^2 value. Specifically, using the new description of the hemodynamic model, six independent parameters were determined by fitting experimental data with the model [Eqs. (1) and (2)], using a built-in fitting procedure in MATLAB (function "*lsqcurvefit*") with the default reconstruction algorithm, which is a trust region reflective algorithm. The reconstruction of the six unknowns was done by searching within a bounded region of the six-parameter space with the input values being the four parameters $|\mathbf{D}|/|\mathbf{O}|$, $|\mathbf{O}|/|\mathbf{T}|$, $\arg(\mathbf{D})$–$\arg(\mathbf{O})$, and $\arg(\mathbf{O})$–$\arg(\mathbf{T})$ (measured at multiple frequencies). Optimal sets of the six unknown

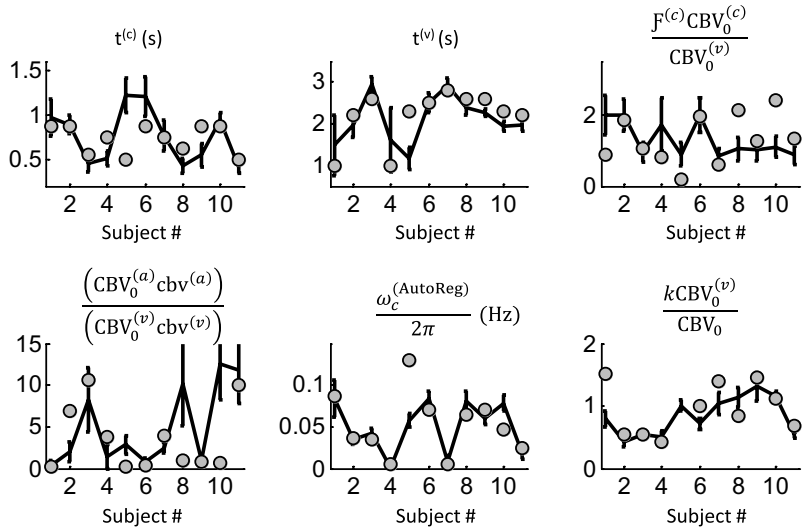

Fig. 2. Results of the fitting procedure for the six parameters of the model, which are $t^{(c)}$, the blood transit time in capillaries, $t^{(v)}$, venous blood transit time, $\mathcal{F}^{(c)}\mathrm{CBV}_0^{(c)}/\mathrm{CBV}_0^{(v)}$, the baseline capillary to venous blood volume ratio, $(\mathrm{CBV}_0^{(a)}\mathrm{cbv}^{(a)})/(\mathrm{CBV}_0^{(v)}\mathrm{cbv}^{(v)})$, the ratio of the arterial to venous blood volume oscillations, $[\omega_c^{(\mathrm{AutoReg})}/(2\pi)]$, autoregulation cutoff frequency, and $k\mathrm{CBV}_0^{(v)}/\mathrm{CBV}_0$, the high-frequency flow-to-volume amplitude ratio (k) coupled with the baseline venous-to-total blood volume. The values of the parameters are reported in terms of their mean value and standard deviation (solid lines). In comparison, the converted set of our previously considered 10 parameters[2] are shown by the gray dots.

Table 1. Summary of the effects of the eight independent model parameters (defined in the text) on the CHS spectral features within the frequency band 0–0.5 Hz.

	Model parameters							
	$S^{(a)}$	α	$t^{(c)}$	$t^{(v)}$	$\frac{\mathcal{F}^{(c)}\mathrm{CBV}_0^{(c)}}{\mathrm{CBV}_0^{(v)}}$	$\frac{(\mathrm{CBV}_0^{(a)}\mathrm{cbv}^{(a)})}{(\mathrm{CBV}_0^{(v)}\mathrm{cbv}^{(v)})}$	$\frac{\omega_c^{(\mathrm{AutoReg})}}{2\pi}$	$\frac{k\mathrm{CBV}_0^{(v)}}{\mathrm{CBV}_0}$
Spectral features (0–0.5 Hz)	0.78–1.00	0.7–0.9 s^1	0.7–0.9 s	1.75–2.25 s	1.85–2.4	0.87–1.12	0.07–0.09 Hz	1–1.29
Phase change of Arg(**D**)–Arg(**O**) (deg)	8.7 ↑	1.5 ↑	−5.5 ↓	5.1 ↑	5.8 ↑	0.5 ↑	4.4 ↑	1.2 ↑
Slope change of Arg(**D**)–Arg(**O**) (deg/Hz)	260 ↑	31 ↑	—	—	64 ↑	20 ↑	−20 ↓	58 ↑
Positive peak amplitude change of Arg(**O**)–Arg(**T**) (deg)	—	3.6 ↑	3.0 ↑	−0.8 ↓	2.2 ↑	−0.5 ↓	−0.7 ↓	3.6 ↑
Negative peak amplitude change of Arg(**O**)–Arg(**T**) (deg)	—	−2.6 ↓	−3.5 ↓	2.5 ↑	—	0.4 ↑	1.2 ↑	−2.9 ↓
Positive peak frequency change of Arg(**O**)–Arg(**T**) (mHz)	—	−2 ↓	−6 ↓	−4 ↓	—	2 ↑	8 ↑	−4 ↓
Zero-crossing frequency change of Arg(**O**)–Arg(**T**) (mHz)	—	—	−18 ↓	−10 ↓	8 ↑	—	18 ↑	—
Value change of $\lvert\mathbf{D}\rvert/\lvert\mathbf{O}\rvert$	—	0.055 ↑	0.044 ↑	—	0.040 ↑	—	−0.017 ↓	0.080 ↑
Peak amplitude change of $\lvert\mathbf{O}\rvert/\lvert\mathbf{T}\rvert$	0.34 ↑	0.12 ↑	0.096 ↑	−0.058 ↓	0.11 ↑	0.028 ↑	−0.044 ↓	0.22 ↑
Peak frequency change of $\lvert\mathbf{O}\rvert/\lvert\mathbf{T}\rvert$ (mHz)	210 ↑	—	−14 ↓	−18 ↓	—	—	18 ↑	—

Note: The arrows indicate whether an increase (↑) or decrease (↓) of each parameter induces the spectral change reported in the left column. Larger arrows indicate a stronger dependence on the parameter with respect to smaller arrows. The values reported in each cell are the differences between the spectral features (listed in the left column) evaluated for the high and low values of the parameter ranges reported on the top row for each parameter. The phase difference, change in phase slope, and change of $|\mathbf{D}|/|\mathbf{O}|$, are the average values over the frequency range 0.05–0.45 Hz.

parameters were found by minimizing a cost function (χ^2), which is the sum of the residuals squared. The upper and lower limits for the parameters in the fitting procedure reflect physiological ranges and are summarized in Ref. 13. We have used 54 different sets of initial guesses for the six unknown parameters, which were evenly spread out throughout the range of upper and lower limits for the parameters. For each initial guess, the solution of the six parameters and the corresponding χ^2 value were stored at each step of the fitting procedure for further analysis. Eventually, the previous solutions for the original 10 model parameters[2] were combined into the new set of 6 independent parameters for comparison.

3. Results

The measured spectra from all eleven subjects of $|\mathbf{D}|/|\mathbf{O}|$, $|\mathbf{O}|/|\mathbf{T}|$, $\arg(\mathbf{D})$–$\arg(\mathbf{O})$, and $\arg(\mathbf{O})$–$\arg(\mathbf{T})$ over the paced breathing frequencies are shown in Fig. 1. The solid black lines correspond to the fitted spectra with the minimum χ^2 value. The shaded gray areas correspond to all other solutions of the six parameters with a slightly greater χ^2 value than the smallest one, so that the fits fall within one standard deviation of the data points.

Since multiple solutions for each subject were obtained by the fitting routine, Fig. 2 shows the average solutions for each of the six parameters, with error bars corresponding to the standard deviation. Since we have analyzed this data set previously with ten unknowns,[2] we have converted the 10 previous parameters into the newly defined six parameters. The converted solutions from our previous results are shown in Fig. 2 by the grey dots. It is noteworthy that the converted solutions for all but one subject (#5) fall within three standard deviations of the six parameter solutions. The 10 parameter solutions, while not unique, can therefore be converted into unique solutions that are consistent with the new data analysis. The only exception is subject #5, where, however, the fit of the data was not as good as the other subjects, especially in the amplitude ratios.

Each of the six parameters of the hemodynamic model influences the shape of the CHS spectra. We have summarized this dependence previously for the 10 parameter solutions.[2] In Table 1 we report the updated summary in terms of the new set of six parameters. Table 1 is a visual summary of the key spectral features and specifies how they are affected by each one of the model parameters within the reported physiological ranges. Large arrows indicate a stronger dependence than that associated with the small arrows. We observe that some of the effects reported in Table 1 do not hold in general but give a guidance and reference for interpreting measured coherent hemodynamics spectra.

4. Discussion

We have analyzed previously collected CHS data during a paced breathing paradigm. We have previously shown that the CHS spectra can be analyzed by the novel hemodynamic model introduced by Fantini.[1,2] The initial description of the model was treating each one of 10 ten model parameters as independent.[2] In particular, baseline concentrations of blood volume in the three compartments as well as the blood volume oscillations in each compartment were assumed to be independent parameters. We have recently demonstrated that this assumption was not correct, but that, instead, the number of independent parameters can be reduced to six, only giving access to ratios of baseline blood volume and oscillations between microvascular compartments. Also, the inverse of the Grubb's exponent, k, is not an independent variable, but rather linked to the venous-to-total blood volume ratio.

Converting the previously obtained results[2] into the new set of six independent parameters showed that the previous results are consistent with the fitting results obtained with the new description (Fig. 2). However, it shall be pointed out that the previous results (gray dots in Fig. 2) were obtained by fitting the data to the hemodynamic model considering also the contributions from the capillary volume oscillations, $\mathbf{cbv}^{(c)}(\omega)$, which have been set to zero in this new formulation. This difference could explain remaining discrepancies between the solutions of the six parameters.

5. Conclusion

The introduction of quantitative photon migration methods and hemodynamic models have played a key role in the effort of translating NIRS measurements into relevant physiological, functional, or diagnostic parameters. The major requirement for such models to be effective is to achieve a good

compromise between (1) their ability to describe the complex structure and biology of tissues and (2) a sufficiently simplified treatment that limits the number of free parameters. In this paper, we have reported the analysis of coherent hemodynamics spectra collected in a paced breathing protocol. This analysis was based on a new hemodynamic model that, while treating the complexity of the cerebral microvasculature,[1] results in a limited number (eight) of independent physiological parameters. This number is smaller than the set of 12 parameters considered in a previous implementation.[2] The 8 independent parameters are the arterial saturation, rate of oxygen transfer from blood to tissue, blood transit time in the capillary and venous compartments, relative capillary-to-venous blood volume ratio, relative arterial-to-venous blood volume changes in response to a hemodynamic challenge, cutoff frequency for cerebral autoregulation, and the product of the high-frequency flow-to-volume amplitude ratio times the venous-to-total blood volume ratio. These model parameters provide a relevant description of the cerebral vasculature, its blood flow, and its dynamic response to physiological or functional perturbations, so that they can be important for a range of functional and diagnostic studies.

Acknowledgments

This research is supported by the National Institutes of Health (Grant No. R01-CA154774) and by the National Science Foundation (Award No. IIS-1065154). The authors J. M. Kainerstorfer and A. Sassaroli have equally contributed to the work.

References

1. S. Fantini, "Dynamic model for the tissue concentration and oxygen saturation of hemoglobin in relation to blood volume, flow velocity, and oxygen consumption: Implications for functional neuroimaging and coherent hemodynamics spectroscopy (CHS)," *Neuroimage* **85**, 202–221 (2014).
2. M. L. Pierro, B. Hallacoglu, A. Sassaroli, J. M. Kainerstorfer, S. Fantini, "Validation of a novel hemodynamic model for coherent hemodynamics spectroscopy (CHS) and functional brain studies with fNIRS and fMRI," *Neuroimage* **85**, 222–233 (2014).
3. M. Ferrari and V. Quaresima, "A brief review on the history of human functional near-infrared spectroscopy (fNIRS) development and fields of application," *Neuroimage* **63**, 921–935 (2012).
4. E. M. Hillman, "Optical brain imaging *in vivo*: Techniques and applications from animal to man," *J Biomed Opt.* **12**, 051402 (2007).
5. D. R. Leff, F. Orihuela-Espina, C. E. Elwell, T. Athanasiou, D. T. Delpy, A. W. Darzi, G. Z. Yang, "Assessment of the cerebral cortex during motor task behaviours in adults: A systematic review of functional near infrared spectroscopy (fNIRS) studies," *Neuroimage* **54**, 2922–2936 (2011).
6. T. Katura, N. Tanaka, A. Obata, H. Sato, A. Maki, "Quantitative evaluation of interrelations between spontaneous low-frequency oscillations in cerebral hemodynamics and systemic cardiovascular dynamics," *Neuroimage* **31**, 1592–1600 (2006).
7. M. Reinhard, E. Wehrle-Wieland, D. Grabiak, M. Roth, B. Guschlbauer, J. Timmer, C. Weiller, A. Hetzel, "Oscillatory cerebral hemodynamics — The macro- vs. microvascular level," *J. Neurol. Sci.* **250**, 103–109 (2006).
8. R. Cheng, Y. Shang, D. Hayes, Jr., S. P. Saha, G. Yu, "Noninvasive optical evaluation of spontaneous low frequency oscillations in cerebral hemodynamics," *Neuroimage* **62**, 1445–1454 (2012).
9. J. A. Claassen, B. D. Levine, R. Zhang, "Dynamic cerebral autoregulation during repeated squat-stand maneuvers," *J. Appl. Physiol.* **106**, 153–160 (2009).
10. A. H. van Beek, J. Lagro, M. G. Olde-Rikkert, R. Zhang, J. A. Claassen, "Oscillations in cerebral blood flow and cortical oxygenation in Alzheimer's disease," *Neurobiol. Aging* **33**, 428 e421–431 (2012).
11. R. Aaslid, M. Blaha, G. Sviri, C. M. Douville, D. W. Newell, "Asymmetric dynamic cerebral autoregulatory response to cyclic stimuli," *Stroke* **38**, 1465–1469 (2007).
12. S. Fantini, "A new hemodynamic model shows that temporal perturbations of cerebral blood flow and metabolic rate of oxygen cannot be measured individually using functional near-infrared spectroscopy," *Physiol. Measure.* **35**, N1–N9 (2014).
13. J. M. Kainerstorfer, A. Sassaroli, B. Hallacoglu, M. L. Pierro, S. Fantini, "Practical steps for applying a new dynamic model to near-infrared spectroscopy measurements of hemodynamic oscillations and transient changes: Implications for cerebrovascular and functional brain studies," *Acad. Radiol.* **21**, 185–196 (2014).
14. J. L. Chen, L. Wei, V. Acuff, D. Bereczki, F. J. Hans, T. Otsuka, W. Finnegan, C. Patlak, J. Fenstermacher, "Slightly altered permeability-surface area products imply some cerebral capillary recruitment during hypercapnia," *Microvas. Res.* **48**, 190–211 (1994).

15. U. Gobel, B. Klein, H. Schrock, W. Kuschinsky, "Lack of capillary recruitment in the brains of awake rats during hypercapnia," *J. Cerebral Blood Flow Metabolism: Official J. Int. Soc. Cerebral Blood Flow Metabolism* **9**, 491–499 (1989).
16. W. Kuschinsky, O. B. Paulson,"Capillary circulation in the brain," *Cerebrovas. Brain Metabolism Rev.* **4**, 261–286 (1992).
17. A. Villringer, "The intravascular susceptibility effect and the underlying physiology of fMRI," *Neuroimage* **62**, 995–999 (2012).
18. A. Villringer, A. Them, U. Lindauer, K. Einhaupl, U. Dirnagl, "Capillary perfusion of the rat brain cortex. An *in vivo* confocal microscopy study," *Circulation Res.* **75**, 55–62 (1994).
19. G. Zoccoli, M. L. Lucchi, E. Andreoli, V. Bach, T. Cianci, P. Lenzi, C. Franzini, "Brain capillary perfusion during sleep," *J. Cerebral Blood Flow Metabolism: Official J. Int. Soc. Cerebral Blood Flow Metabolism* **16**, 1312–1318 (1996).